

Fabrication and Antibacterial Performance of Nano-silver-Doped Monoliths by the Sol-Gel Method

Taymaz Tabari^{a,*}, Davood Beiknejad^b, Haman Tavakkoli^c, Mohammad Habibi Jouibari^a,
Ramin Zafar Mehrabian^a and Mohammad Javad Chaichi^b

^aDepartment of Chemistry, Faculty of Sciences, Gorgan Branch, Islamic Azad University, Gorgan, Iran.

^bFaculty of Chemistry, University of Mazandaran, Babolsar, Iran.

^cDepartment of Chemistry, Science and Research Branch, Islamic Azad University, Khuzestan, Iran.

Received 19 December 2012, revised 29 January 2013, accepted 2 April 2013.

ABSTRACT

The organic-inorganic hybrids of glycine, tetraethylortho silicate (TEOS) and triethylphosphate (TEP) doped with silver ions were prepared by the sol-gel method. After moulding and heating at 600 °C to remove organic compound, porous Ag/P₂O₅-SiO₂ monoliths were obtained. Scanning electron microscopy (SEM), energy dispersive X-ray (EDX) spectrum, transmission electron microscopy (TEM), infrared spectroscopy (FT-IR) and scanning tunnelling microscopy (STM) were used to structurally study monoliths. Surface area, pore volume and swelling degree of the samples were adjusted with different contents of TEP in the starting composition. Ag ions were stably released into the water at 30 °C for 28 days. Antibacterial experimentation revealed that such materials, treated at 600 °C, could restrain *Escherichia coli* effectively.

KEYWORDS

Antibacterial effect, nano-silver, phosphorous, organic-inorganic hybrid, sol-gel.

1. Introduction

Human beings are often infected by microorganisms like bacteria, moulds, yeast, viruses, etc., in their living environment. Research has been intensive in an antibacterial material containing various natural and inorganic substances such as tea extract, caducean, copper, zinc, etc.¹⁻⁷ Among them, silver ions have long been known to have powerful antibacterial properties.⁸⁻¹⁰ Recently, more and more attention has been paid to the problems of environmental pollution and health.^{11,12} In respect of sewage-disposal systems and biomedical applications, development of Ag-doped materials with a long and stable antibacterial period is very desirable. However, antibacterial materials such as zeolites covered with silver ions have only a short antibacterial period¹³. Sol-gel-derived antibacterial silver containing silica glass heated to 900 °C showed silver ion releasing at low concentrations of several ppm for up to 14 days as a probable reason of its compact structure.¹⁴ Silver valence might also be affected by thermal treatment at high temperature to reduce the antibacterial effect. Also, Silver is known for its antibacterial particles and silver nanoparticles are gaining its importance for their antibacterial activity. Silver nanoparticles were found to possess a high surface area compared to bulk atoms which increases the energy, enhancing the antibacterial activity of nanoparticles.^{15,16} In addition, the antibacterial properties of nano-silver-doped filter paper against *Escherichia coli* have been studied.¹⁷ Silver ion release from sol-gel coatings has demonstrated antibacterial activity against *E. coli*.^{18,19} Also, nano-silver-coated fabric inhibited the growth of the Gram-negative bacterium *E. coli*²⁰. In this work, organic and inorganic groups were reacted at the molecular level to form the hybrid; firstly *via* the sol-gel process, and then porous P₂O₅-SiO₂ samples doped uniformly with silver ions were formed by the removal of organic components after a dried gel sample was heated at relatively lower temperature. The

effect of the amount of TEP on the structure, particle size and antibacterial properties of the obtained porous P₂O₅-SiO₂ blocks was investigated.

2. Experimental

Chemicals were purchased from Merck, Aldrich and Fluka chemical companies. The physicochemical characteristics of the monoliths were investigated by the scanning electron microscopy (SEM) and energy dispersive X-ray (EDX) spectrum were recorded using VP-1450, the transmission electron microscopy (TEM) was recorded using LEO-912 AB and scanning tunnelling microscopy (STM) was recorded using (SS1). The structural groups in the samples were characterized by infrared (IR) spectroscopy (Buck 500) using KBr tablets. The Silver valence of the samples was measured by Shimadzu (UV-vis) spectrometer. The release rate of silver ions in water at 30 °C, as a function of soaking time, was carried out by an Ag⁺-selecting electrode using a PHS-3B acidity instrument.

2.1. Preparation of Silver-doped Monoliths

Silver-doped porous P₂O₅-SiO₂ monoliths were prepared by the sol-gel method. TEOS, glycine, TEP, AgNO₃, NH₄OH, DMF and ethanol were used as starting materials. First, TEOS was pre-hydrolyzed in H₂O, DMF, EtOH and ammonium hydroxide solution in the TEOS:H₂O:DMF:NH₄OH:EtOH volume ratio of 1:0.8:0.01:0.005:1.5 at ambient conditions. After stirring vigorously for one hour, different amounts of TEP, according to TEP/TEOS molar ratio in the starting compositions, were mixed with the hydrolyzed sol. Then, glycine, kept at 20 wt% of glycine/(TEOS + TEP), was added to the above solution. Lastly, AgNO₃ was dissolved in the sol under a constant Si/Ag molar ratio of 1/0.01. The obtained sols were kept at 50 °C for gelation and drying. The dried hybrid gels were pulverized into fine powders, moulded into regular blocks, and then

* To whom correspondence should be addressed. E-mail: taymaz_tabari@yahoo.com

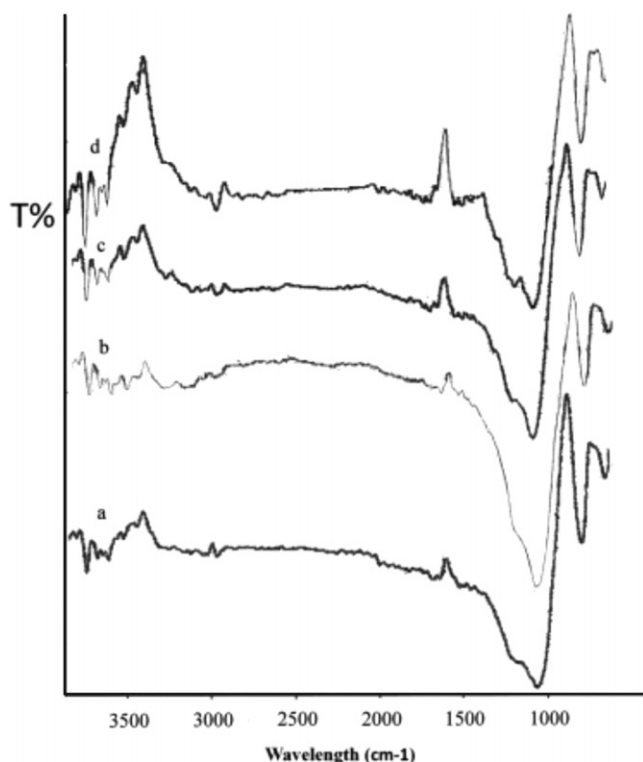


Figure 1 FTIR spectra of the Ag/P₂O₅-SiO₂ monoliths as calcined powders at 600 °C. Composite without phosphorous (a), Composite with 5 % phosphorous (b), composite with 10 % phosphorous (c) and composite with 15 % phosphorous (d).

heat-treated at 600 °C for 6 h to remove organic compounds and residual water. The porous structure was formed after glycine was removed. A small amount of P₂O₅ tended to dissolve in water from the porous structure. Thus, the release rate of silver ions from the samples could be controlled by changing the amount of phosphorous and pore structure.

2.2. Antibacterial Procedure

The antibacterial activity against *Escherichia coli* of Ag-doped P₂O₅-SiO₂ samples were tested by the optical density (OD600) method. Also, phosphate buffer, normal saline solution (17.8 g Na₂HPO₄; 5.5 g NaH₂PO₄; 700 mL distilled water) and 0.5 McFarland *E. coli* were prepared. 0.10 mL g Ag-doped P₂O₅-SiO₂ monoliths were mixed with 70 mL of the above suspension in different flasks. Each flask kept under the same conditions and incubated at 37.8 °C, and 1 mL of each suspension was taken for detection by the optical density (OD600) method. At the same time, a blank sample was obtained by mixing 70 mL PBS and 5 mL *E. coli* suspension for a comparison.

3. Results and Discussion

3.1. Infrared Spectroscopy

Figure 1 shows the infrared spectra of the samples with various TEP/TEOS molar ratios after heating at 600 °C. The broadband at 1077 cm⁻¹ is due to Si-O-Si bonds. The bands at 1100 cm⁻¹ and 1230 cm⁻¹ are due to P-O-Si and P-O-P vibrations, respectively, which indicates that phosphorus can exist in the silica network. The comparison between the IR spectra of monolith without phosphorus (Fig. 1a) and the monoliths contained phosphorus (Fig. 1b–d) show that the band at 1230 cm⁻¹ appeared. Also, these bands showed stronger transmission when the amount of phosphorus increased. It seems, with increasing of the phosphorus

amount in the matrices of silica the band at 1077 cm⁻¹ (Fig. 1a) shows a shift to lower wavelengths (Fig. 1b–d). These results revealed that the phosphorus reacted with silica matrices and the P₂O₅-SiO₂ monolith formed successfully.

3.2. Scanning Electron Microscopy

Figure 2 shows SEM images of P₂O₅-SiO₂ composites in the presence of different initial concentrations of phosphorus. It is found that the surface morphology of the composites is greatly affected by the initial concentration of TEP in the starting solutions. As seen in Fig. 2a, the composite has a smooth surface and the fewest pores, with uniform shapes and sizes existing in every particle. Moreover, each particle irregularly consisted of several much smaller particles. In addition, in Fig. 2b, the morphology of the surface of this composite changed completely with the addition of 5 % phosphorus. Furthermore, in Fig. 2c, 10 % phosphorus composite, the surface morphology shows pores with ordered shape and different size. In Fig. 2d, the surface morphology was changed in the presence of 15 % phosphorus. It seems, the composites with 5 and 15 % phosphorus have a similar surface morphology.

3.3. EDX Analysis

The EDX elemental analysis of the organic-inorganic hybrid was presented in Fig. 3a–d. A substantial peak of Ag was recorded, which confirms the presence of silver in the Ag/Si-O-P. Fig. 3a showed an elemental analysis of the organic-inorganic hybrid without phosphorus. Fig. 3b–d showed the presence of phosphorus in matrices of 5 to 15 % Ag/Si-O-P monolith. The EDX revealed that the P₂O₅-SiO₂ monoliths were prepared by doping of Ag⁺ in a matrix of monoliths.

3.4. Transmission Electron Microscopy

TEM observations of the Ag/P₂O₅-SiO₂ monoliths reveal that most of the silver particles are dispersed within the matrix and that their size distribution is quite narrow, as indicated in Fig. 4. The average size of silver particles was evaluated from measurements on the TEM micrographs to be 5–25 nm. There was a great difference in the average size of the silver particles between the composites in the absence and presence of different amount of phosphorous. In Fig. 4a, the silver distribution is low without phosphorus and the average size is not clear. In Fig. 4b, in which 5 % phosphorous exists in the monolith matrix, the average size is in the range of 10–13 nm, but the distribution of particles is not ordered. On the other hand, in Fig. 4c, with 10 % phosphorous the particle distribution is totally ordered and the average size of silver is in the range of 5–9 nm. In Fig. 4d, with 15 % phosphorous, the average size is in the range of 17–22 nm and the particle distribution is ordered. Furthermore, TEM clearly showed that there were many mesopores and secondary channels between the layers of the composite. These mesopores and secondary channels would increase the surface area of the composite and provide enough space for substrates to access the bioactive sites. This might be one of the main factors of excellent bioactivity and explain the properties of the composites.

3.5. Scanning Tunnelling Microscopy

Figure 5 shows the scanning tunneling microscopy (STM) images (1000 nm × 1000 nm) of composite nanoparticles, which can be used to determine the size and height of particles. In Fig. 5a, in the absence of phosphorous, the bright spots are higher than the dark ones and the distribution of the particles on the surface are mapped in a way that they can be easily identified. Three particles were selected for quantitative measure-

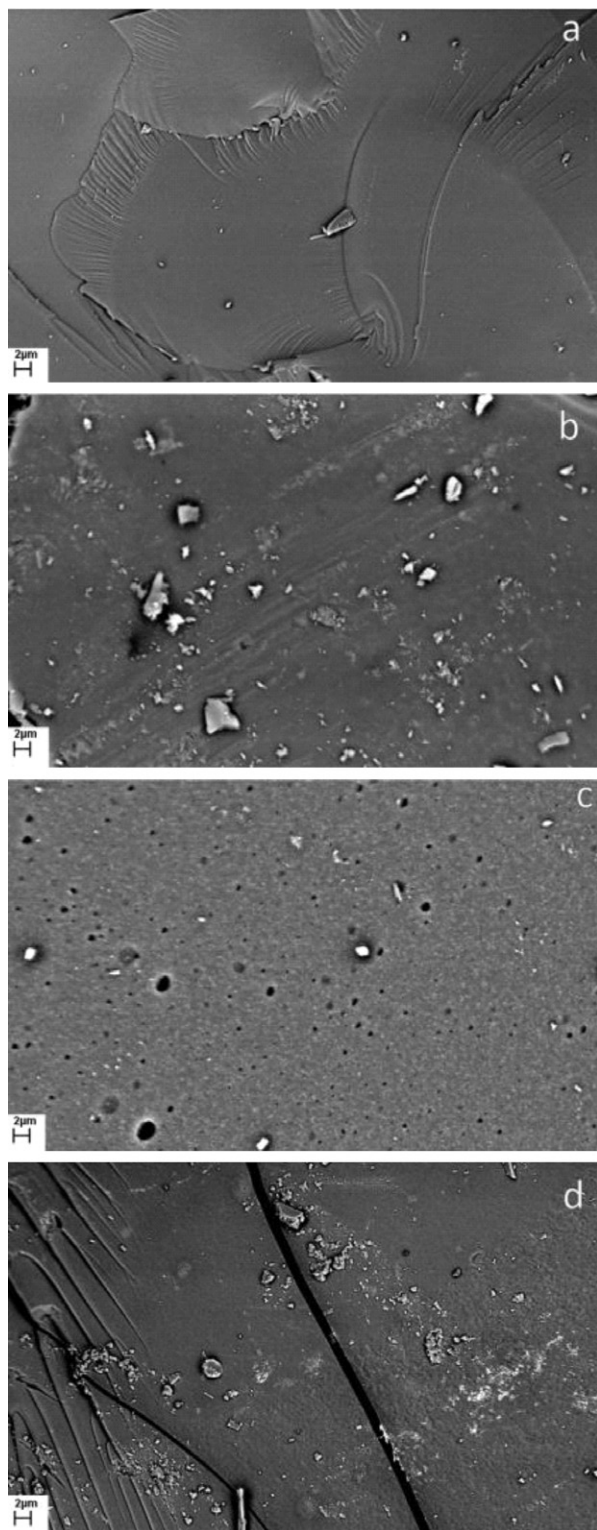


Figure 2 SEM image of calcined $\text{Ag/P}_2\text{O}_5\text{-SiO}_2$ monoliths at $600\text{ }^\circ\text{C}$. Composite without phosphorous (a), composite with 5 % phosphorous (b), composite with 10 % phosphorous (c) and composite with 15 % phosphorous (d).

ments and results showed that their average size and height was approximately 22 nm and 5.8 nm, respectively (Fig. 5b). Also, in Fig. 5c, with 5 % phosphorous, the bright spots are higher than the dark spots when mapped. Three particles were selected for particle size measurements and showed an average size and height of 16 nm and 1.5 nm, respectively (Fig. 5d). In Fig. 5e, in the presence of 10 % phosphorous, the bright dots are higher

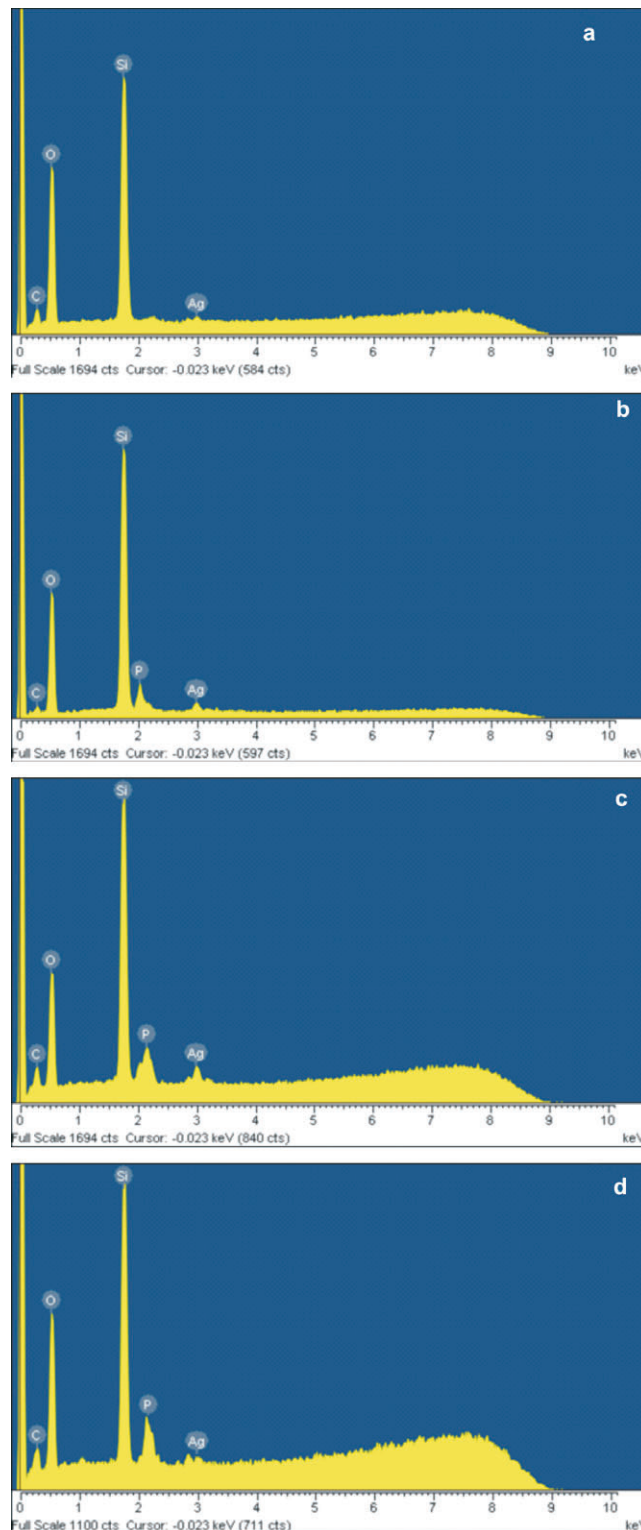


Figure 3 Result of EDX analysis of the $\text{Ag/P}_2\text{O}_5\text{-SiO}_2$ monoliths. Composite without phosphorous (a), composite with 5 % phosphorous (b), composite with 10 % phosphorous (c) and composite with 15 % phosphorous (d).

than dark dots and the distribution of particles on the surface are mapped clearly. Three particles were selected for particle size measurements and the average size and height obtained was around 11 nm and 1.9 nm, respectively (Fig. 5f). In the presence of 15 % phosphorous (Fig. 5g), similar to previous STM figures, five particles were selected for particle size measurements and the average size and height obtained was approximately 17.6 nm

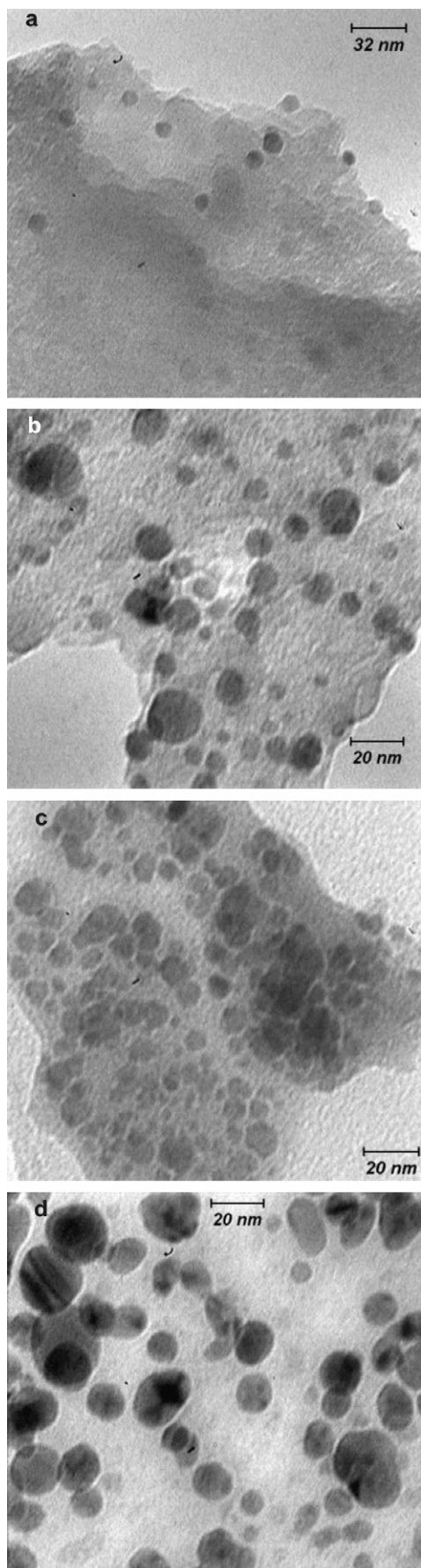


Figure 4 TEM micrograph of calcined $\text{Ag/P}_2\text{O}_5\text{-SiO}_2$ monoliths at $600\text{ }^\circ\text{C}$. Composite without phosphorous (a), composite with 5% phosphorous (b), composite with 10% phosphorous (c) and composite with 15% phosphorous (d).

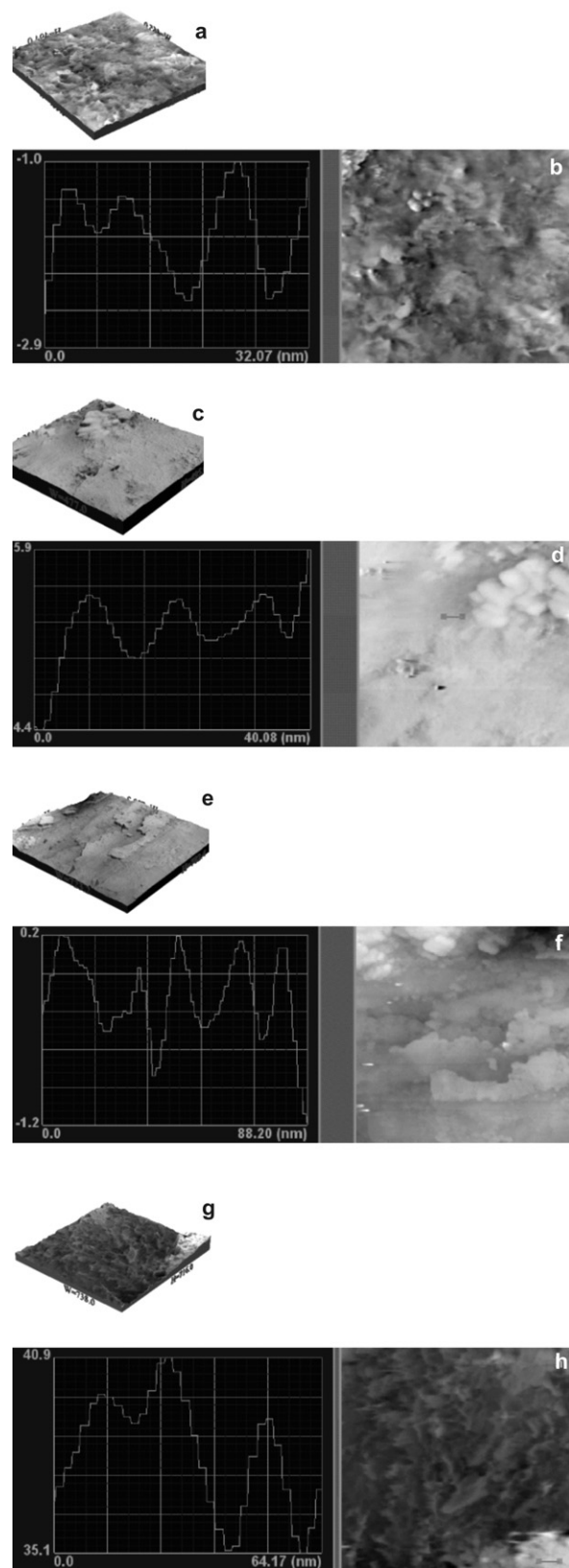


Figure 5 Composite without phosphorous, (a) STM images of $\text{Ag/P}_2\text{O}_5\text{-SiO}_2$ for the area of $1000\text{ nm} \times 1000\text{ nm}$, (b) height profile along the white line. Composite with 5% phosphorous, (c) STM images of $\text{Ag/P}_2\text{O}_5\text{-SiO}_2$ for the area of $1000\text{ nm} \times 1000\text{ nm}$, (d) height profile along the white line. Composite with 10% phosphorous, (e) STM images of $\text{Ag/P}_2\text{O}_5\text{-SiO}_2$ for the area of $1000\text{ nm} \times 1000\text{ nm}$, (f) height profile along the white line. Composite with 15% phosphorous, (g) STM images of $\text{Ag/P}_2\text{O}_5\text{-SiO}_2$ for the area of $1000\text{ nm} \times 1000\text{ nm}$, (h) height profile along the white line.

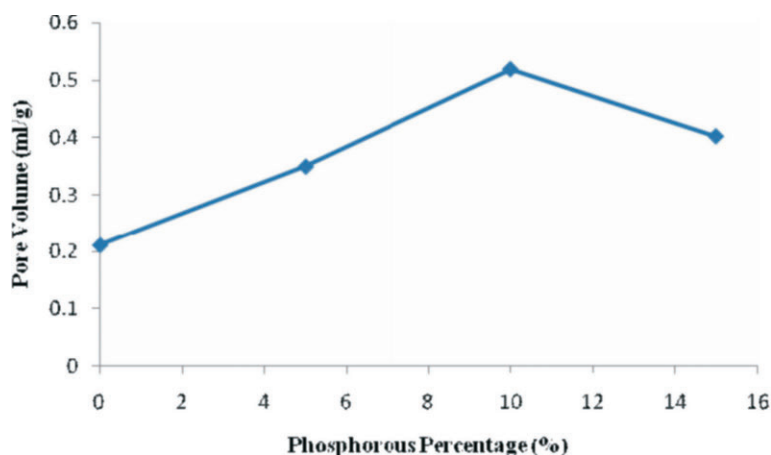


Figure 6 Pore volume of monoliths related to percentage of phosphorous.

and 1 nm, respectively (Fig. 5h). The particle size of composites was reduced as the loading of phosphorous in the matrices of Silica was increased, with the exception of the 15 % case where the average particle size increased in comparison to the 10 % phosphorous composite. Therefore, a relation can be seen between bioactivity and the particle size of composites. When the particle size was reduced, the bioactivity was increased.

On the other hand, as is obvious from the TEM and STM images, the main reason for the difference between the particle size obtained from TEM and STM is the aggregation of the small particles. In the TEM image of the sample without phosphorous, the border between the particles is not clear. Also, when the aggregation is low (15 % phosphorous), the particle size obtained from TEM and STM is the same.

3.6. Degree of Swelling and Pore Volume

In addition to SEM studies, the degree of swelling was also measured as percentage weight variation of monoliths after keeping them for 24 h in dimethylformamide (DMF). The pore volume of monoliths was determined by recording variation in weight (W_t) and comparing to initial weight (W_0). These monoliths were kept in DMF for 24 hours and the pore volume was determined using the density (ρ) of DMF in the following equation:

$$\text{Pore volume} = \frac{W_t - W_0}{W_0 \rho}$$

Figure 6 shows pore volume degree of monoliths; this figure shows that the pore volume was related to phosphorous percentage in the matrices of monoliths. Pore volume was the least in the monolith without phosphorous. However, pore volume increased by increasing the amount of phosphorous in

the media of the monolith. However, pore volume decreased in the monolith with 15 % phosphorous, equalling the pore volume of the 5 % phosphorous. The increase in the amount of phosphorous in the matrix of the monolith is due to the monolith density increasing, as shown in the SEM photograph; the monolith with 10 % phosphorous has a mesoporous structure of 6 to 80 nm. The results revealed that the pore volume is increased as the particle size becomes smaller.²¹ Also, the particle size of the sample with 5 % phosphorous is smaller than the sample with 15 % phosphorous. It seems the sample with 15 % phosphorous has cracks on the surface, which are responsible for increasing the pore volume of this monolith. Interestingly, these results showed a relation between the antibacterial effect and the pore volume obtained with the presented method. Furthermore, the high pore volume of the monolith with 10 % phosphorous had excellent antibacterial activity.

3.7. Release Speed of Silver Ions

Figure 7 shows the release speed of silver ions as a function of soaking time at 30 °C in water up to 28 days. It was detected that a large amount of silver ions was released into the water slowly and steadily if the TEP/TEOS was 10 mol%. The sample with a molar ratio of TEP/TEOS = 15 % showed a better releasing performance. However, a steady release speed of silver ions is much more important than releasing performance for antibacterial applications.

3.8. Antibacterial Properties

A bacterial inhibition growth curve was used to study the growth kinetics of *E. coli* with prepared biocidal samples (Fig. 8).

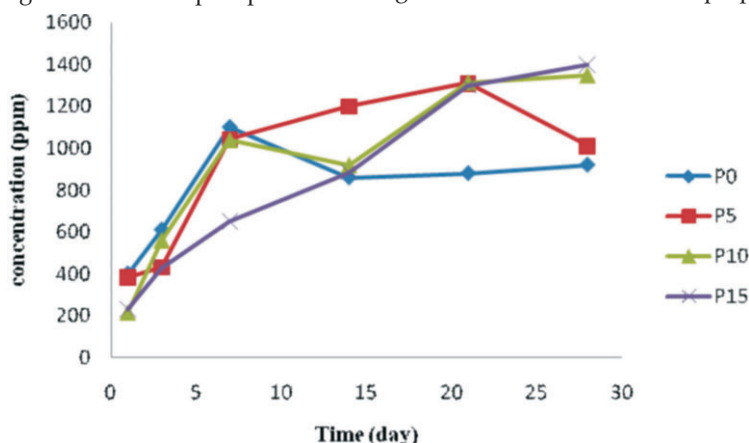


Figure 7 Release speed of silver ions as a function of soaking time at 30 °C.

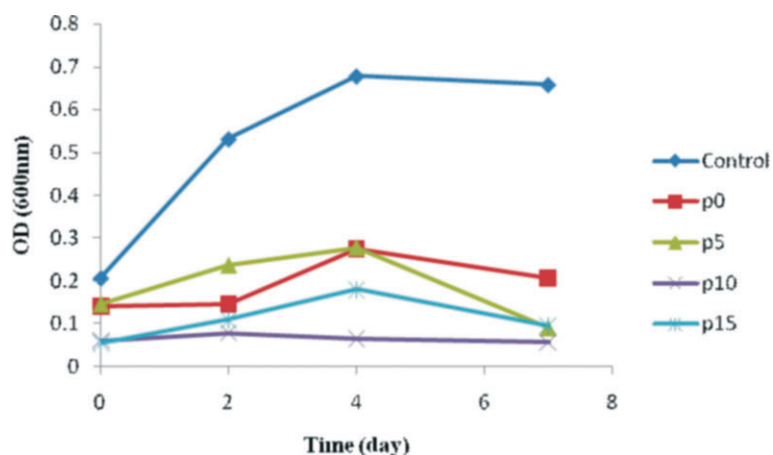


Figure 8 Bacterial growth curve in the presence of silver ions immobilized in Si-O-P monolith was added to the *E. coli* culture. The growth of the bacteria was monitored by measuring the optical density at 600 nm.

The optical density was measured at 600 nm (OD₆₀₀) to monitor bacterial growth; 0.5 McFarland of *E. coli* was grown, then equal amounts (g) of the monoliths, with various concentrations of phosphorous, were added to the bacterial solution. The results showed that the bacterial growth was delayed when the concentration of phosphorous in the monoliths was increased, but the rates of bacterial growth delay were different. The growth of *E. coli* was completely inhibited by the Ag/P₂O₅-SiO₂ monolith when the concentration of phosphorous was 10 %. In addition, Ag/P₂O₅-SiO₂ monolith with 5 % phosphorous concentration was able to slow the growth of *E. coli*. These results confirmed that the Ag/P₂O₅-SiO₂ monolith possessed enhanced antibacterial activity when compared to silver sulfadiazine (SSD). Both silver ions and doped silver ions exhibit antibacterial properties *via* similar mechanisms, such as interactions with bacterial membranes or binding with metabolic materials. However, for the all silver-doped monoliths, the silver ions in Ag/P₂O₅-SiO₂ monolith exhibited significantly higher antibacterial effects than the silver ions in SSD.²² When the silver ions come into contact with bacteria,

precipitates are formed and the antibacterial ability of SSD deteriorates. In contrast, the Ag/P₂O₅-SiO₂ monolith releases silver ions slowly and steadily, which come into contact with bacteria without precipitation. Therefore, the prepared monoliths that contained silver ions showed higher bactericidal efficacy than SSD, which contained only silver ions.²³ These results indicate that the antibacterial efficacy of doped silver ions may depend on the aggregation degree. As the doped silver ions released slowly, which are well dispersed in solutions, exhibited much higher bactericidal activity compared to silver ions with severe aggregation. Also, the nanometer sized monoliths provided a large surface area for more effective antibacterial performance. Furthermore, the antibacterial efficacy of the samples with different TEP/TEOS molar ratios is shown in Fig. 9.

Figure 9 shows a photographic image of the bacterial inhibition of *E. coli*. Among the samples studied, the best results were shown in the sample with 10 % phosphorus (Fig. 9d). On the other hand, in samples without phosphorus, bacterial growth stopped in the first two days (Fig. 9b). Also, after a few days, a

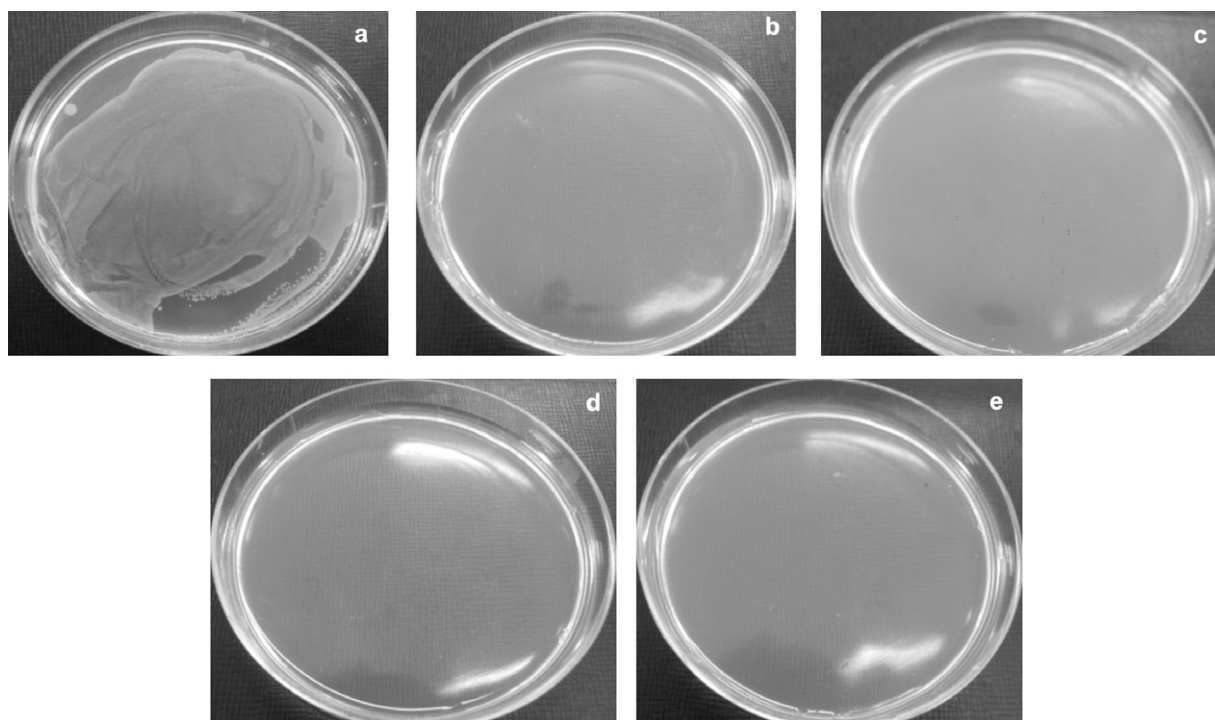


Figure 9 Antibacterial activity of silver-doped monoliths against *E. coli* growth. (a) Absence of Ag⁺ ions, (b) monolith without phosphorous, (c) monolith with 5 % phosphorous, (d) monolith with 10 % phosphorous, (e) monolith with 15 % phosphorous.

gradual increase of bacterial growth is detected *via* optical density (OD600). In the absence of phosphorous, Ag⁺ were precipitated by the rapid release of silver ions in the first seven days (Fig. 7). This shows a decreased concentration of silver ions in the solution. Thus, the concentration of bacteria increased in the last three days (Fig. 8). Furthermore, the antibacterial properties are related to the size of the silver in the matrices of monoliths. Moreover, samples containing 5 % and 15 % phosphorus showed desirable antibacterial properties. Initially, bacterial growth slightly increases, but after four days *E. coli* growth stopped. Both monoliths reduced antibacterial activity to a similar extent after seven days (Fig. 8). The control sample revealed that the *E. coli* grew in the absence of a monolith, clearly showing the antibacterial effect of the synthesized monoliths. The results exhibit the presence of phosphorous due to the slow release and long time effect of the Ag/P₂O₅-SiO₂ organic-inorganic hybrid. Furthermore, the monolith with 10 % phosphorous showed excellent bioactivity throughout. This monolith completely restrained *E. coli* growth in our experiment.

4. Conclusion

The Sol-gel method was successfully used to synthesize a silver-doped organic-inorganic hybrid. Ag⁺ ions existed in the samples after they were heated to 600 °C and phosphorus ions were combined into the silica network. It is confirmed that a large amount of silver ions can be released slowly and steadily into 30 °C water for up to 28 days, which is beneficial to the application. The embedded silver ions exhibited a lower tendency towards aggregation when compared with colloidal silver ions. The fabricated Ag/P₂O₅-SiO₂ monolith had enhanced antibacterial activities against Gram-negative *E. coli* due to the bactericidal properties of the silver ions being immobilized by the P₂O₅-SiO₂ monolith. These results suggest that the Ag/P₂O₅-SiO₂ monolith has potential for use in biofilms, as well as hygienic and anti-adhesion applications.

Acknowledgement

This work was financially supported by project number 51733-890921010 from Islamic Azad University, Gorgan Branch, Iran.

References

- 1 Y. Sung-Chul, O. Seong-Geun and J. Hyung-Jun, *Biomater.*, 2003, **24**, 4921–4928.
- 2 P. Westerhoff and T. Benn, *Environ. Sci. Technol.*, 2008, **42**, 4133–4139.
- 3 L. Ross, R.Y. Surampalli, J. Kim, Z. Hu, K.K. Deng and O. Choi, *Water Res.*, 2008, **42**, 3066–3074.
- 4 B.A. Akgun, N.P. Mellott and C. Durucan, *J. Sol-Gel Sci. Technol.* 2012, **62**, 240–251.
- 5 H.H. Cheng, C.C. Hsieh and C.H. Tsai, *Aerosol Air Qual. Res.*, 2012, **12**, 405–415.
- 6 T. Ivanova, A. Harizanova, T. Koutzarova and B. Vertruyen, *Crystal Res. Technol.*, 2012, **47**, 579–584
- 7 R. Subasri, R. Malathi, A. Jyothirmayi and N.Y. Hebalkar, *Ceram. Int.*, 2012, **38**, 5731–5740
- 8 R. Jayakumar, M. Prabakaran, K. Shalumon and K.P. Chennazhi, *Adv. Polymer Sci.*, 2011, **246**, 263–282.
- 9 H. Miyoshi, H. Ohno, K. Sakai, N. Okamura and H. Kourai, *J. Colloid Interface Sci.*, 2010, **345**, 433–441.
- 10 A. Venugopal, M. Subrahmanyam and M. Pratap, *Water Res.*, 2007, **41**, 379–386.
- 11 G.C. Delgado, *Technol. Soc.*, 2010, **32**, 137–144.
- 12 J. Fu, J. Ji, D. Fan and J. Shen, *J. Biomed. Mater. Res., Part A*, 2006, **79**, 665–674.
- 13 X. Zhang, J. Yan, H. Ni and Y. Cai, *Colloid. Surface A*, 2011, **375**, 186–192.
- 14 K. Yamamoto, S. Tsuneyama, F. Miyaji, H. Kozuka, T. Kokubo and M. Kawashita, *Biomater.*, 2000, **21**, 393–398.
- 15 A. Dwivedi and K. Gopa, *Colloid. Surface A*, 2010, **369**, 27–33.
- 16 K.P. Bankura, D. Maity, M.M.R. Mollick, D. Mondal, B. Bhowmick, M.K., Bain, A. Chakraborty, J. Sarkar, K. Acharya and D. Chattopadhyay, *Carbohydr. Polym.*, 2012, **89**, 1159–1165.
- 17 R. Tankhiwale and S.K. Bajpai, *Colloid. Surface B*, 2009, **69**, 164–168.
- 18 H.J. Jeon, S.C. Yi and S.G. Oh, *Biomaterials*, 2003, **24**, 4921–4928.
- 19 N. Stobie, B. Duffy, D.E. McCormack, J. Colreavy, M. Hidalgo, P. McHale and S.J. Hinder, *Biomater.*, 2008, **29**, 963–969.
- 20 H.Y. Lee, H.K. Park, Y.M. Lee, K. Swan and S.B. Park, *Chem. Comm.*, 2007, **28**, 2959–2961.
- 21 K.J.A. Raj and B. Viswanathan, *Indian J. Chem.*, 2009, **48A**, 1378–1382.
- 22 H. Kong and J. Jang, *Langmuir*, 2008, **24**, 2051–2056.
- 23 T. Klaus, R. Joerger and C.G. Granqvist, *Adv. Mater.*, 2000, **12**, 407–409.